Annu. Rev. Fluid Mech. 1998. 30:507–38

TURBULENT FLOW OVER HILLS AND WAVES

S. E. Belcher
Department of Meteorology, University of Reading, P.O. Box 243, Reading, RG6 6BB, United Kingdom; e-mail: s.e.belcher@reading.ac.uk

J. C. R. Hunt
DAMTP, Silver Street, University of Cambridge, Cambridge, CB3 9EW, United Kingdom; e-mail: ah209@damtp.cam.ac.uk

KEY WORDS: environmental fluid mechanics, atmospheric boundary layer, nonhomogeneous terrain, air–sea interaction, geophysical turbulence

ABSTRACT

This is a review of the mechanisms that control neutrally stable turbulent boundary-layer flow over hills and waves, their relative magnitudes, and how they exert their greatest effects in different regions of the flow. We compare calculations based on various analytical and computational models with each other and with relevant experimental data. We discuss practical applications of these studies.

1. FLUID MECHANICAL AND PRACTICAL ASPECTS

The psalmist's line "I will lift up mine eyes unto the hills from whence cometh my help" (Psalms 121) is relevent to students of complex turbulent flows. This is because turbulent boundary-layer flows over hills and waves are both controlled by mechanisms that are active in many other perturbed turbulent flows. Study of these fluid-dynamical problems contributes to our fundamental understanding of mechanisms that control distorted flows and helps to answer practical environmental and engineering questions.

Twenty years of research in this field has led to general concepts and formulae that have become broadly understood, so much so that they have now been applied in several other disciplines:

1. Atmospheric flows are significantly accelerated over the tops of hills even when the maximum slopes are quite small, because shear in the approaching

0066-4189/98/0115-0507$08.00

wind amplifies this acceleration (Jackson & Hunt 1975). For example, even if the slope of the hill is $\frac{1}{5}$ then the wind speed at the crest is faster by a factor of about $\frac{1}{2}$. This speed-up factor is now incorporated into estimation of wind energy and wind loads on structures on hill tops and other exposed sites (Building Research Establishment 1989; Troen & Petersen 1989).

2. The bulk effect of flow over hills is to increase the drag of the surface on the large-scale atmospheric motion. It is remarkable that this effect only began to be introduced into numerical weather prediction (NWP) in about 1986, when the computational grid became sufficiently refined for this extra drag to be significant. The first steps involved introducing only the drag produced by lee waves generated by stable stratification in the troposphere and stratosphere (Palmer et al 1986). The need to incorporate into NWP the orographic drag from neutrally stable atmospheric boundary-layer flow over hills was recognized only very recently (Mason 1985, Taylor et al 1989), and has led to about a 4% reduction in the root-mean-square (rms) error of forecasts of mean sea-level pressure for three-day weather predictions (Milton & Wilson 1996). This is significant because typically it is the progress in NWP expected over two years.

3. Some of the mean streamlines in the accelerating wind over hills approach the hill surface, whereas others may recirculate in wake regions. Furthermore, turbulence in the flow is greatly changed by hills, especially in the wake. Together these changes to the mean flow and turbulence affect mixing and exchange processes. Examples include (*a*) heat and mass transfer at the surface (Raupach et al 1992, Hewer & Wood 1998); (*b*) precipitation from rain clouds (Carruthers & Choularton 1983, Choularton & Perry 1986); and (*c*) dispersion, deposition and chemical transformation of pollutants (Berlyand 1972, Castro & Snyder 1982). All these effects are beginning to be represented in mesoscale numerical models used for detailed environmental studies (e.g. Pielke 1984, p. 456; Hunt et al 1991). These studies have been extended to the more difficult problem of the transport of sand particles over sand dunes to improve understanding and quantitative modeling of the shapes and bulk movement of sand dunes (e.g. Barndorff-Nielson & Willetts 1991).

4. Research and forecasting models of ocean waves have been guided by Miles's (1957) theory of wave generation by the wind and by Hasselmann's (1962) theory of weakly nonlinear transfer of energy between waves of different wavelength (e.g. Komen et al 1994), but with little relation to ideas or methods of calculating wind over hills, or the resulting drag. Recently,

however, these two fields have begun to converge, as we explain in this review. Current 24-hour forecasts of ocean waves typically have global rms errors of 0.6 m (Fuller & Kellett 1997), which is about 15–20% of the rms wave height. These errors increase systematically when large waves are forecast, when the waves are not forced locally by wind, and when the mean wind conditions are changing.

In fluid dynamical terms, the special and interesting feature of turbulent boundary-layer flow over hills and waves is that the boundary layer is distorted over a horizontal length scale, L, that is comparable to, or shorter than, the depth of the boundary layer, h, so that a large fraction of the depth of the boundary layer does not have time to come into equilibrium during the distortion. This means that special care is needed in modeling the turbulent stresses, as explained in Section 2. The basic structure of the broadly unidirectional boundary-layer flow is maintained over the hill or wave, but the dynamical balance is disturbed enough that significant changes occur to the mean wind (Section 2.4), the turbulence (Section 5), and the processes dependent on the flow, such as the drag (Section 7).

In this paper we explain how various aspects of the changes in the flow over hills and waves are different in different parts of the flow by identifying the largest terms in the equations governing the mean dynamics and the main mechanisms and time scales that govern perturbations to the turbulence. We also review the ways in which various approaches to modeling these aspects are being used for research and for practical problems involving environmental flows. Our review highlights the aspects of the subject where progress has been made, and also areas where there remain controversy and limited understanding.

2. STRUCTURE AND MODELING FLOW OVER A HILL

Upstream of the hill is the *basic flow*, which is taken to be a fully developed, neutrally stratified turbulent boundary layer flowing along the x-axis over level homogeneous terrain. Basic-flow profiles are chosen to model the steady unidirectional surface layer of the atmospheric boundary layer, where the velocity profile, $U_B(z)$, is logarithmic, namely

$$U_B(z) = \frac{u_*}{\kappa} \ln(z/z_0). \quad (1)$$

Here $\kappa \approx 0.4$ is the von Karman constant, z_0 is the roughness parameter, and $u_*^2 = \tau_B(z_0)$ defines the friction velocity, u_*, in terms of τ_B the Reynolds shear stress (Panofsky 1974). Pressure and Reynolds stresses are all normalized on density, which therefore does not appear in equations here. The logarithmic velocity profile needs minor modification at upper levels when the horizontal length scale of the hill is comparable with the boundary-layer depth (Taylor 1977).

The hill is described by $z_s = Hf(x)$, with height H and half length L (defined to be the distance for the hill height to drop to half its maximum height), and produces perturbations to the basic flow, denoted here by Δu, Δw, Δp, and $\Delta \tau$ for the horizontal and vertical velocity perturbations and the pressure and Reynolds shear stress perturbations. The length of the hill is small enough (less than about 10^4 m) that effects of the Earth's rotation are negligible. We focus here mainly on two-dimensional ridges, with no variation in the y-direction. For three-dimensional effects see Mason & Sykes (1979) and Hunt et al (1988). A sketch of the flow geometry is shown in Figure 1.

To accommodate boundary conditions at the surface of the hill, it is convenient to use a transformed vertical coordinate. Jackson & Hunt (1975) used a terrain-following vertical coordinate, defined by

$$Z = z - z_s, \tag{2}$$

near the surface and a Cartesian coordinate, z, far aloft. For ease of explanation, this approach will be followed here because the governing equations then retain their familiar forms, but at the expense of using different coordinate systems in different parts of the flow. For numerical studies (e.g. Gent & Taylor 1976, Newley 1985, Wood & Mason 1993, Burgers & Makin 1993) it is more convenient to use a terrain-following coordinate, Z', that follows the hill surface near

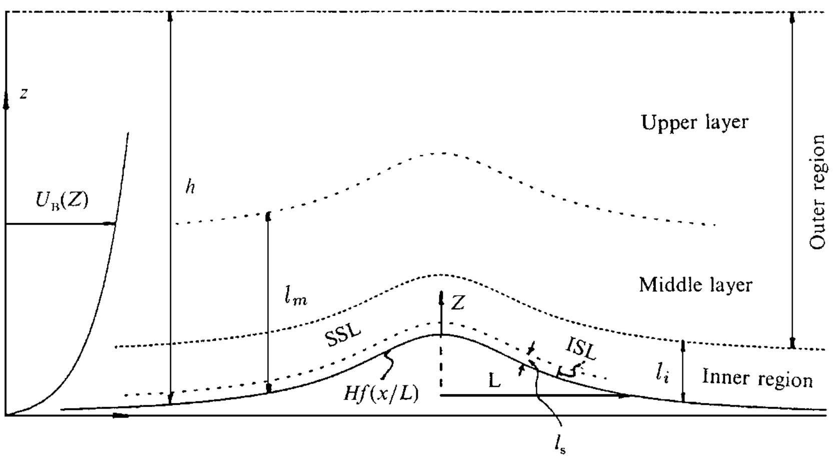

Figure 1 Flow geometry and asymptotic structure for flow over a hill.

the ground and tends smoothly to horizontal far above, e.g. defined by

$$Z' = \frac{z - z_s}{1 - z_s/D}, \tag{3}$$

where D is the depth of the computational domain. Additional Jacobian terms then appear in equations for the perturbed flow. A further, and more economical, approach is to use a streamline coordinate system, (x, η), so that

$$z = \eta + \delta(x, \eta), \tag{4}$$

where $\delta(x, \eta)$ is the displacement of the mean streamline from the horizontal. In the recast equations of motion, $\delta(x, \eta)$ then becomes the dependent variable (Miles 1993).

For hills with *low slopes*, so that $H/L \ll 1$, perturbations to the basic flow are small enough that $\Delta u/U_B\,(L) = O(H/L) \ll 1$, and they can be calculated using linearized equations, with products of perturbations neglected, namely

$$\begin{aligned} U_B \frac{\partial \Delta u}{\partial x} + \Delta w \frac{dU_B}{dz} &= -\frac{\partial \Delta p}{\partial x} + \frac{\partial \Delta \tau}{\partial z} \\ U_B \frac{\partial \Delta w}{\partial x} &= -\frac{\partial \Delta p}{\partial z} + \frac{\partial \Delta \tau}{\partial x} \\ \frac{\partial \Delta u}{\partial x} + \frac{\partial \Delta w}{\partial z} &= 0. \end{aligned} \tag{5}$$

There are also linear terms in the momentum equations involving normal Reynolds stresses, $\Delta\tau_{11} = -\Delta\overline{u'^2}$ and $\Delta\tau_{33} = -\Delta\overline{w'^2}$, but they play no significant dynamical role (Townsend 1972, Jackson & Hunt 1975) and so are neglected here.

The mean wind speed is zero at the hill surface ($z = z_s + z_0$, where z_0 is the roughness of the surface), and all perturbations decay far above the hill; hence

$$\Delta u = \Delta w = 0, \quad \text{on } z = z_s + z_0; \qquad \Delta u, \Delta w \to 0 \quad \text{as } z/L \to \infty. \tag{6}$$

The air flow over the hill can be calculated once the Reynolds stress perturbation, $\Delta\tau$, has been modeled. This important issue is discussed next.

2.1 *Time Scales of the Distortion to the Turbulence*

The undisturbed boundary layer is a very slowly changing turbulent flow, and so can be approximately modeled throughout its depth using turbulence models based on eddy-transfer concepts, such as an eddy-viscosity model. However, changes to the boundary layer induced by the hill occur over short length and time scales, which invalidates the use of such an eddy-viscosity model throughout the flow (as also demonstrated, in engineering contexts, by Launder 1989).

Hence in this and other distorted turbulent flows it is instructive to define two time scales: one that characterizes distortion of the turbulence by the mean flow, and another that characterizes relaxation of the turbulence to equilibrium with the surrounding mean-flow environment. The ratio of these time scales then gives a measure of how far the turbulence is from local equilibrium (Britter et al 1981) and thence provides guidance toward suitable turbulence models.

First, the advection time scale, T_A, characterizes the time for turbulent eddies to be advected and distorted by the mean flow over the hill:

$$T_A = \frac{L}{U_B + \Delta u} \approx \frac{L}{U_B}\left\{1 + O\left(\frac{\Delta u}{U_B}\right)\right\}, \quad \text{when } H/L \ll 1. \tag{7}$$

On this time scale, turbulent eddies in the air flow are distorted by straining motions associated with perturbations to the mean flow caused by the hill.

Second, the Lagrangian integral time scale, T_L, characterizes the decorrelation and relaxation time scale of the large energy-containing eddies, and it scales as the ratio of the smallest integral length scale, L_x, to the corresponding rms velocity scale (Tennekes & Lumley 1972, Ch. 2). In a boundary layer near a surface the turbulence is anisotropic and the vertical integral length scale, $L_x^{(w)}$, is smallest because it is constrained by the boundary, so that $L_x^{(w)} \approx \kappa Z$. The appropriate velocity scale for the eddying motions is then the vertical-velocity variance, which is $(\overline{w'^2})^{\frac{1}{2}} \approx 1.3u_*$ in the surface layer (Panofsky 1974). The Lagrangian time scale can then be estimated to be

$$T_L = \kappa Z/u_*. \tag{8}$$

On this time scale the energy-containing eddies are also dissipated, and the turbulence comes into equilibrium with the surrounding mean-flow velocity gradient (Tennekes & Lumley 1972, Ch. 3).

2.2 *Regions of the Flow*

In *local-equilibrium regions* of the flow, $T_L \ll T_A$, and turbulent eddies adjust to equilibrium with the surrounding mean-flow velocity gradient before they are advected over the hill; hence an eddy viscosity can be used to relate the Reynolds stress perturbations to the local mean-velocity gradient (Townsend 1961). By contrast, in *rapid-distortion regions*, $T_L \gg T_A$, and the mean flow advects turbulent eddies over the hill more rapidly than they interact nonlinearly. Hence, local properties of the turbulence are determined by distortion of the upstream turbulence by the cumulative mean strain, which is described by rapid-distortion theory (Batchelor & Proudman 1954, Hunt 1973) (see also Section 5).

Now, T_A decreases and T_L increases with height, and they are comparable at heights $Z \sim l_i$, where

$$l_i \ \ln(l_i/z_0) = 2\kappa^2 L. \tag{9}$$

The coefficient on the right, $2\kappa^2$, is chosen to be consistent with Jackson & Hunt's (1975) estimate from the mean-momentum equation. For practical purposes, in the range $10^4 < L/z_0 < 10^7$, l_i can be estimated explicitly by $l_i/z_0 = \frac{1}{8}(L/z_0)^{0.9}$. Flow over hills can then be divided into two regions (Figure 1): a local-equilibrium region near the surface, $Z < l_i$, where $T_L < T_A$, which has been called the *inner region*; and a rapid-distortion region, $Z > l_i$, where $T_A < T_L$, which has been called the *outer region*. In most practical applications the length of the hill is sufficiently large compared with the roughness that $\ln(L/z_0) \gg 1$, so that $l_i/L \sim 1/\ln(l_i/z_0) \ll 1$ and the inner region is a thin layer. For a typical case wherein $L = 500$ m and $z_0 = 0.1$ m, the inner-region height is $l_i \approx 28$ m.

The ratio T_A/T_L has the same magnitude as the ratio of the rate of dissipation of turbulent kinetic energy, ε, to the advection of turbulent kinetic energy, $U_B \partial q/\partial x$, and so the regions of the flow can be identified from the relative magnitudes of the terms in the turbulent kinetic energy equation. Figure 2 (Belcher et al 1993) shows profiles of these terms at the top of an isolated hill computed using the second-order closure model of Launder et al (1975), which includes approximations to all the terms, namely advection, production, transport, and dissipation of turbulent kinetic energy. Noting the logarithmic scale, the results are consistent with the physical interpretations of the inner and outer regions given above, showing how production balances dissipation in the lower part of the inner region ($Z \lesssim \frac{1}{2}l_i$), and how production balances advection of turbulent kinetic energy in the outer region ($Z < l_i$). All terms are of comparable magnitude where $Z \sim l_i$. If the Reynolds-stress equations are considered, curvature of the mean streamlines also has a significant effect on the stress perturbations at levels $Z \sim l_i$ (Zeman & Jensen 1987).

2.3 *Modeling the Turbulent Stress*

These ideas can now be drawn together to identify appropriate modeling of turbulent stresses. Consider first zonal models, whereby different turbulence models are used in different regions. Eddy-viscosity models are appropriate when used only in the inner region and when the slope of the hill is small. Following Townsend (1961), the mixing-length model is then a useful approximation to the Reynolds shear stress, so that for hills of low slope perturbations to the shear stress, $\Delta\tau$, are given by

$$\Delta\tau = 2\kappa u_* Z \partial \Delta u/\partial Z. \tag{10}$$

In the outer region, turbulent eddies are advected over the hill in a time that is too small for them to transport significant momentum, so that perturbations to the Reynolds stress have a negligible effect on the perturbed mean flow (see Section 2.4). The perturbation shear stress can therefore be set to zero when

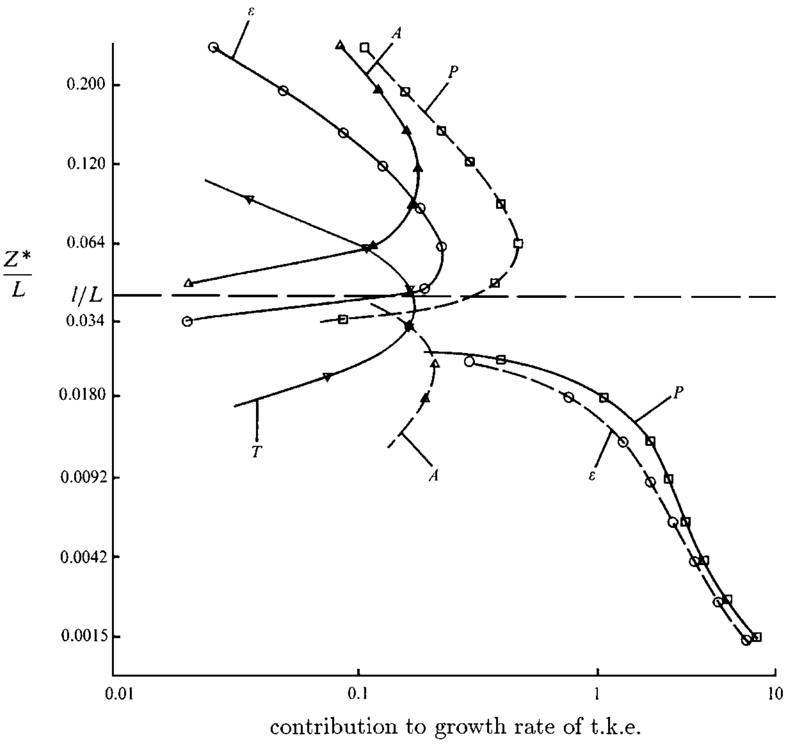

Figure 2 Balance of terms in the turbulent kinetic energy equation integrated from far upstream to the summit of an isolated hill and normalized on u_*^3/L. *Solid lines* denote positive quantities, *dashed lines* negative quantities. *P*: integrated production rate; *A*: integrated advection; *T*: integrated transport; ε: integrated dissipation rate. (From Belcher et al 1993.)

calculating the mean flow. Perturbations to the turbulence in this region are discussed in Section 5.

In an analytical model, Belcher et al (1993) used the mixing-length model in the inner region and set the perturbation stress gradients to zero in the outer region (a *truncated mixing-length model*). This procedure actually leads to small, but non-zero, stress perturbations far above the hill, and so does not satisfy the boundary condition that $\Delta\tau \to 0$ as $z/L \to \infty$. Harris et al (1995) and van Duin (1997) introduce damping functions so that the eddy viscosity, and hence $\Delta\tau$, decay smoothly to zero in the outer region and show that the vertical scale of the damping can affect results. Although this approach approximates decay of the Reynolds stresses between the inner and outer regions, it does not explicitly model the particular physical processes that occur in this intermediate zone.

More general models for the turbulent stress should describe the limiting behaviors in the inner and outer regions in one model valid over the whole flow. Full second-order closure models are one possibility, as used for example in the computations of Newley (1985) or Mastenbroek (1996), who both used the second-order closure of Launder et al (1975), or in the computations of Zeman & Jensen (1987). A less general method that is appropriate for weakly perturbed turbulent boundary layers is to calculate the shear stress from an equation based on the turbulent kinetic energy equation with the assumption that the ratio of the shear stress to the turbulent kinetic energy is constant (e.g. Bradshaw et al 1967, Townsend 1972, 1980, Miles 1993). Effects of advection of the shear stress in the outer region are then correctly modeled; in contrast the more common $k-\varepsilon$ model fails badly in the outer region because it is based on an eddy viscosity (Belcher et al 1993).

2.4 *Scaling Changes to the Mean Flow*

Now that the model for the Reynolds stress has been decided, scaling analysis shows how the dynamical balances in the momentum equations change in the different regions of the flow, which then illustrates the structure of linear perturbations to flow over hills of low slope.

In the outer region, where $z \gtrsim l_i$ and in the present discussion the Cartesian coordinate z is used, the turbulence is distorted rapidly so that $\Delta\tau/u_*^2 \sim \Delta u/U_B(L) = O(H/L)$ (Britter et al 1981). The ratio of the perturbation stress gradient to mean-flow advection in the x-momentum equation (Equation 5) is then

$$\frac{\partial\Delta\tau/\partial z}{U_B\partial\Delta u/\partial x} \sim \frac{(H/L)u_*^2/L}{U_B(L)(H/L)U_B(L)/L} \sim \left(\frac{u_*}{U_B(L)}\right)^2. \tag{11}$$

In the atmospheric boundary layer, $u_*/U_B(L)$ is typically in the range 0.03–0.07, and so the perturbation stress gradient is negligible in the outer region, with only very small corrections. If an eddy-viscosity model is used erroneously in the outer region, then, although the outer region remains inviscid at leading order, the small stress gradients, which are of $O(u_*/U_B(L))$ relative to the advection terms (Jacobs 1987, van Duin & Janssen 1992), affect the pressure and thence the drag on the hill (see Section 7).

The dynamics in the outer region are analyzed by considering first an *upper layer*, where $z \sim L$ and the curvature of the basic velocity profile is small, i.e. $d^2U_B/dz^2 \ll U_B(L)/L^2$. The perturbed flow then reduces to potential flow, so that Δw is described by Laplace's equation, $\nabla^2\Delta w = 0$ (Jackson & Hunt 1975). Solutions show that, at the crest of the hill, Δu, $\Delta w \sim U_B(L)H/L$, and $\Delta p \sim -U_B^2(L)H/L$. Toward the surface, the curvature of the basic logarithmic velocity profile needs to be accounted for. In this *middle* *layer*, where $z \sim l_m$, with l_m defined by $d^2U_B/dz^2|_{z=l_m} = U_B(l_m)/L^2$, the vertical velocity is governed by the Rayleigh equation (Hunt et al 1988), namely

$$\left(\nabla^2 - \frac{U_B''}{U_B}\right)\Delta w = 0. \tag{12}$$

Perturbations in the middle layer are then inviscid, but rotational. When $L = 500$ m and $z_0 = 0.1$ m, $l_m = 180$ m. When the hill is very long, the middle-layer extends to the top of the boundary layer. At the crest of a hill, Δw increases with height through the middle layer, whereas it decreases in the upper layer; Δu decreases with height through both layers, with a more rapid decrease in the middle layer.

In the *inner region*, where $Z \sim l_i$ and in the present discussion the displaced coordinate Z is used, perturbations to the shear stress can be estimated using the mixing-length model (Equation 10). The detailed solutions show that shear in the perturbation velocity scales as $\partial\Delta u/\partial Z \sim (\Delta u/l_i)l_i/L$, because the perturbed velocity is approximately logarithmic. On using Equation 10, the ratio of the perturbation stress gradient to mean-flow advection in the x-momentum equation (Equation 5) is then estimated to be

$$\frac{\partial\Delta\tau/\partial Z}{U_B\partial\Delta u/\partial x} \sim \frac{(2\kappa u_* l_i \partial\Delta u/\partial Z)/l_i}{U_B(l_i)\Delta u/L} \sim \frac{u_*}{U_B(l_i)}. \tag{13}$$

Hence the perturbation stress gradient remains small compared with the mean-flow advection at leading order. But at first order in $u_*/U_B(l_i)$, both the stress terms and the inertial terms associated with the mean-velocity gradient have to be retained, and the perturbed flow is controlled by the boundary-layer equations (Hunt et al 1988). The combination of these effects means that the maximum velocity perturbation is $\Delta u \sim U_B(L)\{U_B(L)/U_B(l_i)\}^2 H/L$, which occurs at the crest of the hill at $Z \approx l_i/3$, with small variation with z_0/L. Above this height, over the crest of the hill, the velocity perturbation decreases in proportion to $1/U_B\,(z)$. Some authors have redefined the thickness of the inner region phenomenologically to be the height of the maximum velocity perturbation (see the discussion in Walmsley & Taylor 1996).

Very near the surface, $\partial\Delta\tau/\partial Z$ becomes large, and there is a new balance in the momentum equation with the shear stress perturbation important at leading order (Sykes 1980). In this *inner surface layer* (Hunt et al 1988) the perturbation stress is constant with height and the perturbation streamwise velocity tends to a logarithmic profile. The depth of this layer, l_s, can be estimated by $l_s \sim (l_i z_0)^{\frac{1}{2}}$ (Hunt et al 1988), which gives $l_s \approx 1.7$ m if $l_i = 28$ m and $z_0 = 0.1$ m; it is a very thin layer.

3. INTERACTIONS BETWEEN THE INNER AND OUTER REGIONS

Stewartson (1974) and Messiter (1979) first identified the mechanisms that couple flow between the inner and outer regions of laminar boundary layers. The same concepts can be applied to turbulent boundary layers, but as is now shown, the magnitudes are different.

Accordingly, consider the displacement of a streamline, $\delta(x,z)$, which for hills of low slope is related to the vertical velocity by $\Delta w = U_B\, d\delta(x,z)/dx$. The displacement at the top of the inner region, written as $\delta(x)$, is caused by (*a*) displacement over the hill itself; (*b*) a Bernoulli displacement associated with the horizontal pressure gradient that develops in the upper layer; (*c*) the effects of mean shear in the middle layer; and (*d*) frictional effects of the shear stresses in the inner region. Now, in the upper layer the perturbed flow is approximately irrotational, so that Δw is determined by Laplace's equation with the boundary conditions that Δw tends to zero far aloft, far upstream and downstream of the hill, and that at $z \sim l_m$ the condition is $\Delta w = U_B\, d\delta(x,l_m)/dx \approx U_B\, d\delta(x)/dx$ because $\delta(x,z)$ remains nearly constant with height through the middle layer. Hence the vertical velocity and thence also the horizontal pressure gradient in the upper layer are determined by $\delta(x)$. But the horizontal pressure gradient in the upper layer is equal, at leading order, to the horizontal pressure gradient in the inner region, because the middle layer and inner region are both thin. This horizontal pressure gradient in the inner region then accelerates flow in the inner region and so changes $\delta(x)$, which then further affects the upper-layer pressure gradient: Hence there is a coupling.

To estimate the magnitude of $\delta(x)$, consider first the vertical velocity, which is given by the continuity equation (Equation 5 transformed into displaced coordinates), so that at the top of the inner region, $Z \sim l_i$,

$$\Delta w(Z \sim l_i) = U_B(l_i) H \frac{df}{dx} - \int_{z_0}^{l_i} \frac{\partial \Delta u}{\partial x} dZ. \tag{14}$$

Now $\partial \Delta u/\partial x$ can be estimated using the x-momentum equation (Equation 5 transformed into displaced coordinates)

$$U_B(l_i)\frac{\partial \Delta u}{\partial x} = -\frac{\partial \Delta p}{\partial x} + \frac{\partial \Delta \tau}{\partial Z} + \text{inertial shear terms.} \tag{15}$$

The inertial shear terms lead only to small corrections to the Bernoulli contribution to displacement of streamlines and so are not considered futher here. Since the inner region is thin, $l_i \ll L$, the pressure is approximately constant with height there. Hence combining Equations 14 and 15 shows that $\delta(x)$ can be expressed as a sum of effects:

$$\delta(x) \simeq Hf(x) + l_i \frac{\Delta p}{U_B^2(l_i)} + \delta_\tau(x), \tag{16a}$$

namely, displacement by the hill itself, the Bernoulli variation of streamline height associated with pressure variations, and the displacement caused by the surface shear stress, which is given by

$$\delta_\tau(x) = \frac{1}{U_B^2(l_i)} \int_{-\infty}^{x} \Delta\tau(x', z_0)dx'. \tag{16b}$$

So, how does $\Delta\tau(x, z_0)$ vary in relation to the outer-region flow? As is well known from classical boundary-layer theory, Equation 5 shows that at the surface, where $Z = z_0$, the stress gradient is

$$\partial\Delta\tau/\partial Z|_{Z=z_0} = \partial\Delta p/\partial x|_{Z=z_0}. \tag{17}$$

But to determine how $\Delta\tau(x, z_0)$ varies with Δp or $\partial\Delta p/\partial x$, we need to consider how $\Delta\tau$ varies with Z. Differentiating Equation 15 with respect to Z and multiplying by $2\kappa u_* Z$ leads to an approximate equation for $\Delta\tau$ in the inner region, namely

$$U_B(l_i)\frac{\partial\Delta\tau}{\partial x} \approx 2\kappa u_* Z \frac{\partial^2\Delta\tau}{\partial Z^2}, \tag{18}$$

which shows that $\partial^2\Delta\tau/\partial Z^2$ becomes large as $Z/l_i \to 0$ (Sykes 1980). By integrating Equation 18 over x and Z and using Equation 17, Hunt & Richards (1984) show that $\Delta\tau(x, z_0)$ is related to $\Delta p(x, z_0)$ by

$$-\Delta p(x, z_0) = \frac{U_B(l_i)}{2\kappa u_*} \int_{z_0}^{l_i} \frac{\Delta\tau(x, Z)}{Z} dZ \approx \frac{\ln^2(l_i/z_0)}{2\kappa^2} \Delta\tau(x, z_0). \tag{19}$$

By contrast, in a high Reynolds number laminar flow, where $\Delta\tau = \nu\partial\Delta u/\partial Z$, it follows from Equation 5 that $\partial^2\Delta\tau/\partial Z^2|_{Z=z_0} = 0$, and so $\partial\Delta\tau/\partial Z$ varies only slowly through the inner region. Hence, on using Equation 17, the surface stress is estimated to be

$$\Delta\tau(x, z_0) \simeq -\int_{z_0}^{l_i} \frac{\partial\tau}{\partial Z} dZ \simeq -l_i \frac{\partial\tau}{\partial Z}(x, z_0) = -l_i \frac{\partial\Delta p}{\partial x}(x, z_0). \tag{20}$$

Comparing Equations 19 and 20 (which are strictly valid only for hills with low slopes, $H/L \ll 1$, and small roughness, $\ln(L/z_0) \gg 1$) shows how, when the flow is turbulent, the surface shear-stress perturbation tends to be in phase with, and proportional to, the surface pressure perturbation. But when the flow is laminar with high Reynolds number, the surface stress perturbation tends to be approximately in phase with the surface pressure gradient (Hunt & Richards 1984). The result, (Equation 19) is broadly applicable to many boundary-layer flows from aerofoils to bluff bodies (where the slopes are certainly not small) as shown by the experimental results of Achenbach (1968), and it helps indicate where boundary layers separate, as explained in Section 6.

Return now to the original question of estimating the magnitude of the streamline displacement at the top of the inner region $\delta(x)$. It follows from Equation 16*b* and Equation 19 that for turbulent flows

$$\delta_\tau(x) \sim \frac{1}{U_B^2(l_i)} \frac{2\kappa^2}{\ln^2(l_i/z_0)} \int_{-\infty}^{x} \Delta p(x, z_0)dx$$
$$= O\left(l_i \frac{H}{L} \frac{1}{\ln(l_i/z_0)} \frac{U_B^2(L)}{U_B^2(l_i)}\right). \tag{21}$$

The inviscid Bernoulli contribution to the displacement is of order

$$l_i \frac{\Delta p}{U_B^2(l_i)} = O\left(l_i \frac{H}{L} \frac{U_B^2(L)}{U_B^2(l_i)}\right). \tag{22}$$

Hence $\delta_\tau(x)$ is smaller than the Bernoulli contribution by a factor of $\ln^{-1}(l_i/z_0) \ll 1$. This explains why the inviscid analysis of the outer region is, to the first approximation, independent of $\delta_\tau(x)$ and the effects of shear stresses in the inner region. Although small, $\delta_\tau(x)$ is significant because it is asymmetric about the crest of the hill, with streamlines being displaced closer to the surface on the upwind side than on the downwind side, and leads to a net drag force on hills and waves, as explained in Section 7.

In contrast, for high Reynolds number laminar flow, the shear stress leads to a displacement calculated from Equation 16*b* and Equation 20 given by

$$\delta_\tau(x) \sim \frac{1}{U_B^2(l_i)} \int_{-\infty}^{x} l_i \frac{\partial \Delta p}{\partial x'} dx' = l_i \frac{\Delta p(x, z_0)}{U_B^2(l_i)} = O\left(l_i \frac{H}{L} \frac{U_B^2(L)}{U_B^2(l_i)}\right), \tag{23}$$

which is of the same order as the Bernoulli term. Hence in the laminar flow the coupling between the inner and outer regions is much stronger (Benjamin 1959, Smith et al 1982).

4. SPECIAL FEATURES OF FLOW OVER MOVING WAVES

Suppose now that the surface carries a sinusoidal traveling wave, $\zeta' = \mathrm{Re}\{a \exp\{ik(x' - ct')\}\}$, which has complex phase speed $c = c_r + \mathrm{i}c_i$, so that it propagates at speed c_r and its amplitude grows at rate kc_i. The characteristic horizontal length scale is $L = k^{-1}$ and $H = a$. Turbulent flow over

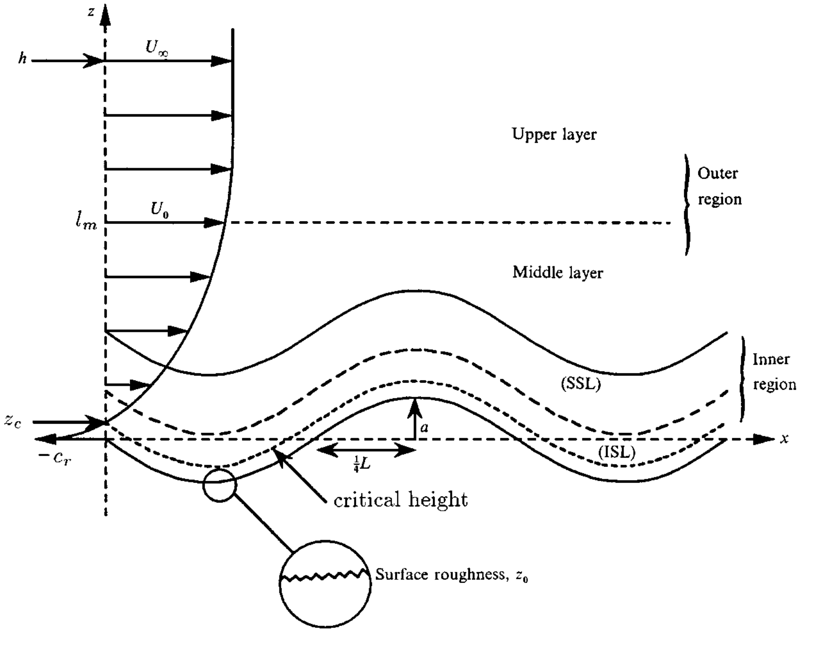

Figure 3 Flow geometry and asymptotic structure for flow over a wave viewed as moving with the wave crests.

such waves has similarities and also differences with flow over rigid stationary undulations (such as a range of hills), which can be clarified by studying the flow in a frame moving at the wave speed, c_r, when the wave surface and basic velocity become $\overline{\zeta} = a \exp\{ik(x - ic_i t)\}$ and $\overline{U}_B = U_B - c_r$ (Figure 3).

4.1 *Effects of the Critical Layer*

When the wind and waves propagate in the same direction, the wind speed, $\overline{U}_B$, is zero at height z_c, called the *critical height*, which has both kinematical and dynamical consequences. Following Phillips (1977, p. 121), the kinematical effect can be understood by considering the displacement of streamlines, $\delta(x, z)$, which is given by

$$\delta(x, z) = \int^x \frac{\Delta w}{\overline{U}_B + \Delta u} \mathrm{d}x'. \tag{24}$$

Hence, for waves of low slope, $\delta(x, z)$ is largest at the critical height where $\overline{U}_B$ is zero. Local analysis of the mean stream function in the vicinity of the critical height shows that there are closed streamlines centered at the crest of the wave at the critical height, as sketched in Figure 4. If the wave is growing,

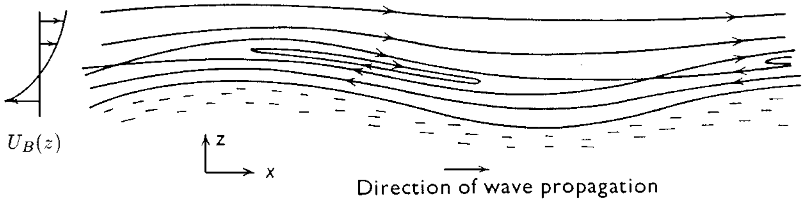

Figure 4 Mean streamlines of flow over waves viewed as moving with the waves. The closed loops are centered at the critical height and shifted downwind of the crest for a growing wave. (From Phillips 1977.)

then the centers of the closed streamlines move downstream of the crest by $kx \sim c_i/U_B(L)$. The thickness of the region of closed mean streamlines can be estimated from the local analysis to be

$$l_c \sim (4\Delta w(z_c)/k\bar{U}_B'(z_c))^{\frac{1}{2}}. \tag{25}$$

In a turbulent flow, the critical-layer streamlines represent only the weak mean flow because fluid elements are rapidly advected across the critical layer by the turbulent eddies.

Changes in Δu across the critical height have a dynamical effect on the whole perturbed flow. Linear stability analysis of a sheared boundary layer over a flat rigid surface shows that there can be growing propagating modes centered on the critical height, as illustrated in Prandtl (1960, p. 115). A surface wave traveling along a water surface can force a coupled motion in the air and water, both propagating at the same speed, namely the eigenvalue c_r. Hence the surface wave could force an unstable shear mode in the air, which then grows and induces growth of the water wave. The first thorough analysis of this mechanism was by Miles (1957), who assumed that the critical height was sufficiently high that the turbulent stress could be neglected, i.e. in our terminology the critical height is in the outer region. Given this assumption, Miles (1957) argued that the airflow perturbations are described by the unsteady Rayleigh equation, which contains the key term $\bar{U}_B''/(\bar{U}_B - \mathrm{i}c_i)$, as in Equation 12. Clearly, unless the wave amplitude varies with time, i.e. $c_i \neq 0$, the equation is singular at z_c. By solving the inviscid equations above and below the air–water interface and by matching the vertical velocity and pressure at z_c, Miles (1957) calculated c_i in the limit $c_i/u_* \to 0$ from the resulting eigenvalue relationship. Lighthill (1962) suggested a physical interpretation of how redistribution of vorticity over the growing wave leads to a "vortex force" and hence wave growth. Over long times of $O(\rho_w/\rho_a)$ wave periods, the growing wave extracts momentum from the air flow and reduces the curvature of the wind profile until this mechanism is quenched (Janssen 1982). These analyses leave unanswered questions about the role of turbulent stress near the critical layer or near the boundary. Mastenbroek (1996) commented that none of the numerical studies of turbulent air flow over slowly growing waves, $c_i/u_* \ll 1$, demonstrated dynamical effects of a critical layer directly.

4.2 *Scaling the Distortion to the Turbulence*

Following Belcher & Hunt (1993), Mastenbroek (1996), and Cohen (1997), effects of a traveling wave on the turbulence in the air flow can be estimated using an extension of the scale analysis developed for the flow over hills, in Section 2. The main difference in flow over waves is that the advection speed by the mean wind relative to the wave is $\bar{U}_B = U_B - c_r$, which is negative below the critical height. The time scale over which the eddies are distorted is defined to remain positive by using the magnitude of the advection speed so that $T_A = k^{-1}/|U_B(Z) - c_r|$. The Lagrangian time scale remains the same to leading order, namely $T_L = \kappa Z/u_*$, because the basic flow over the wave is a surface layer (e.g. Phillips 1977, Section 4.10). Hence, over a propagating wave, $T_L \sim T_A$ at heights $Z \sim l_i$, where l_i is given implicitly by

$$kl_i \,|\ln(l_i/z_0) - \kappa c_r/u_*| = 2\kappa^2. \tag{26}$$

Solutions of Equation 26 for l_i vary with c_r/u_*, as shown in Figure 5. When c_r/u_* is smaller than a bifurcation value, $(c_r/u_*)_b \approx 23$ when $kz_0 = 10^{-4}$, there is just one solution to Equation 26. The structure of the air flow is then similar to flow over hills, namely, a local-equilibrium *inner region* near the surface, $z < l_i$, which contains the critical height, and a rapid-distortion *outer region* in $z > l_i$. Hence the Reynolds stress can be modeled using approaches similar to those used in flow over hills. As c_r/u_* increases, the critical height moves away from the wave surface and, because mean-flow advection is small in the vicinity of the critical height, the inner region thickens.

When $c_r/u_* > (c_r/u_*)_b$, there are three solutions to Equation 26. But the flow can again be considered to have a two-layer structure with an inner region, $z < l_i$, whose depth is given by the smallest solution to Equation 26, and an outer region, $z > l_i$, which now contains the critical height surrounded by the other two solutions to Equation 26 (Figure 5). Turbulence modeling follows as for slow waves, with the additional observation that fluid elements do not spend long enough in the critical layer to come into a local equilibrium (Phillips 1977, p. 121), so that rapid-distortion effects need to be accounted for there. As c_r/u_* increases, mean-flow advection near the surface relative to the wave increases, and the inner-region depth reduces, so that $kl_i \sim 2\kappa u_*/c_r$.

4.3 *Wind–Wave Regimes*

Figure 5 provides a conceptual framework for classifying air flow over water waves and suggests that it may be useful to consider three parameter regimes.

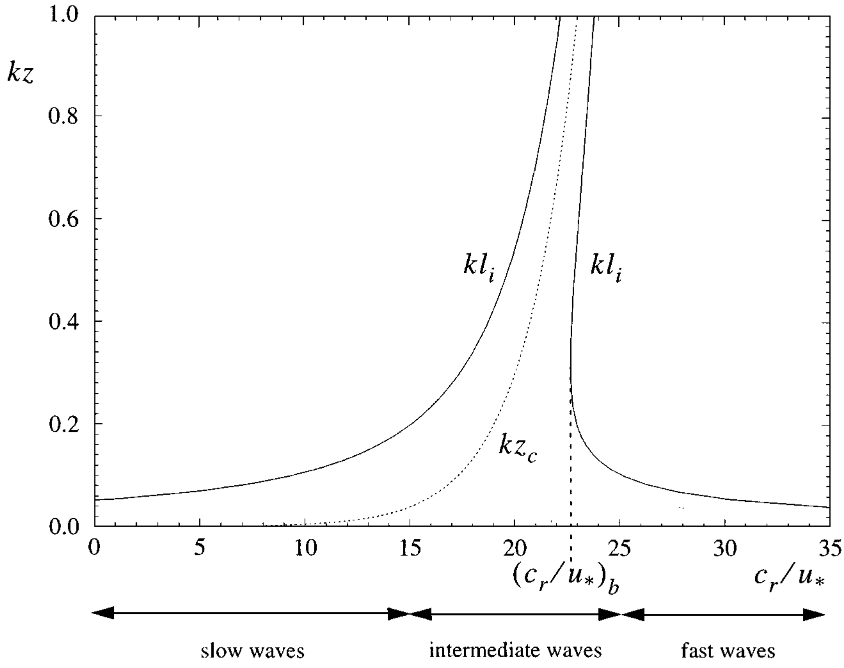

Figure 5 Variation with c_r/u_* of solutions for the normalized inner-region height, kl_i, and critical height, kz_c, when $kz_0 = 10^{-4}$. For given c_r/u_*, an inner, local equilibrium region lies between $kz = 0$ and the smallest value of kl_i, and an outer, rapid-distortion, region lies above. *Solid lines*: kl_i; *dotted lines*: kz_c.

Slow waves have $c_r/u_* \lesssim 15$, so that $kl_i \ll 1$. The critical height then lies in the inner surface layer and plays no significant dynamical role. The air flow perturbations are similar to flow over a stationary undulation, but effectively with roughness z_c and small corrections to the velocity of $O(akc_r\, kl_i)$ owing to the orbital motions at the wave surface (Belcher & Hunt 1993). Asymmetry in the flow is then similar to asymmetry in flow over a hill described in Section 3, but with z_c and $\overline{U}_B$ replacing z_0 and U_B in Equation 21.

Intermediate waves lie in the range $15 \lesssim c_r/u_* \lesssim 25$, so the inner region is thick, $kl_i \sim 1$, and the critical height lies in $l_i \lesssim z_c \lesssim k^{-1}$. The critical layer and the inner region are not then distinct, and the details of their interaction remain to be elucidated. We anticipate that, as c_r/u_* increases from the slow regime, the reverse flow below the critical height becomes stronger and produces a "negative" asymmetric displacement of streamlines, i.e. upwind of the crest, while above the critical height the asymmetric displacement is positive, i.e.

downwind of the crest as for slow waves. The critical-layer mechanism probably also displaces streamlines downwind of the crest. Hence we expect that, as c_r/u_* increases across the intermediate regime, the asymmetric component of the flow reaches a maximum and then decreases to zero.

Fast waves lie in the range $c_r/u_* \gtrsim 25$, so that $c_r/U_B(L) \gtrsim 1$, and the critical layer is far above the surface, $kz_c \gtrsim 1$, and so plays no significant dynamical role. Flow over the wave is therefore largely against the wave, and there is "negative" asymmetry from sheltering. Orbital motions at the water surface force additional air-flow perturbations ($\Delta u, \Delta w \sim akc_r kl_i \sim aku_*$) that contribute comparable negative asymmetries (Mastenbroek 1996, Cohen 1997).

5. DISTORTION OF VORTICITY AND THE STRUCTURE OF TURBULENCE

We now turn to effects of hills and waves on the large energy-containing turbulent eddies, which are affected by linear processes through rapid distortion in the outer regions. In addition, weakly nonlinear processes can reorganize mean-flow vorticity to produce new large-scale circulations.

As explained in Section 2, in the rapid-distortion regions $T_A \ll T_L$, so that vortex lines, and thence vorticity of the energy-containing eddies $(\omega_x, \omega_y, \omega_z)$, are primarily distorted by anisotropic straining by the mean flow (Batchelor & Proudman 1954). Over the top of a hill or wave, $\omega_x \propto \Delta u$ and is increased, while $\omega_z \propto (U_B + \Delta u)^{-1}$ is decreased; the turbulence intensity then changes, so that, if u_0 is the intensity in the upstream boundary layer, $\Delta\overline{u'^2}/u_0^2$ and $\Delta\overline{w'^2}/u_0^2$ are of order $\Delta u(x, z)/U_B(z)$ (Britter et al 1981). These rapid-distortion estimates agree reasonably well with laboratory data (Britter et al 1981, Gong et al 1996, Mastenbroek et al 1996) and field experiments (Mason & King 1985, Zeman & Jensen 1987). The asymmetric displacement of the inner layer (Equation 21) leads to an asymmetric component of the outer-region flow and thence to small asymmetric changes to the intensities (Sykes 1980). Changes to the normal stresses caused by rapid distortion do also occur in the inner region but are usually neglected in leading-order analyses (Townsend 1980, Belcher et al 1993). The rapid-distortion changes to the intensities, and also to the shear stress, are much smaller, by a factor $u_*/U_B(z)$, than estimates obtained using the mixing-length model (Belcher et al 1993). Mason & King (1985) also measured spectra and showed that distortion of the energy-containing eddies, with wavenumbers of order z^{-1}, agrees broadly with rapid-distortion theory based on the strain at height z; however, the largest-scale eddies, with wavenumbers smaller than z^{-1}, impinge on the surface of the hill, and their associated horizontal and vertical velocity fluctuations $\tilde{u}$ and $\tilde{w}$ behave like a slowly varying basic flow, so that we expect $\Delta\tilde{u} \propto \Delta u$.

When the basic flow is perpendicular to the crests of ridges, a secondary mean flow can grow exponentially through an inviscid instability. Analyses of Craik (1982) and Phillips et al (1996) show that a perturbation velocity that varies with wavenumber k_2 in the spanwise direction, namely $\mathbf{u}^{(s)}(\mathbf{x}, t) = e^{\sigma t} e^{\mathrm{i}k_2 y} \hat{\mathbf{u}}(z)$, interacts with the mean flow over the hills. The vertical component of vorticity ω_z increases exponentially through a Stokes drift of $O(H/L)^2$, whereby the net vertical stretching of ω_z on the upwind slope exceeds the net shortening over hill tops. The resulting net vorticity has a vertical scale of the order of the wavelength of the ridges, L. Exponential growth of the streamwise vorticity, ω_x, is produced by the rotation and stretching of ω_z by the mean shear. This explanation (Phillips et al 1996) is consistent with wind-tunnel measurements of Gong et al (1996), which show oscillations in the streamwise mean velocity in the spanwise direction on a scale comparable to the wavelength of the hills.

When the hill slopes are steep enough to cause separation, there are other causes of cellular structure and streamwise vortices (as described in Section 6). Also, persistent longitudinal vortices occur in turbulent boundary layers over flat surfaces: According to Townsend's (1976, Section 7.20) stability analysis, these are driven by mean perturbations in the normal stresses. Over hills the normal stresses are, on average, larger than over flat surfaces, which suggests that this mechanism is even more likely to be initiated over hills. In natural boundary layers, streamwise vortices can also develop on Coriolis time scales driven by wind shear, which is larger for larger surface drag (Mason & Sykes 1980). The resulting streamwise vortices have vertical scale comparable with the boundary layer depth, h, i.e. greater than L.

In tropical and semi-arid countries, the turbulence over hills and sand dunes driven by thermal convection can be more energetic than the shear-driven turbulence. The eddies are then larger and impinge on the surface, i.e. $L_x^{(w)} \sim z$, for $z \lesssim h/5$, cf. $L_x^{(w)} \sim \kappa z$ for shear-driven turbulence. Interaction between the hill and turbulence can then lead to a different kind of circulating motion. For example, in the limit of weak mean flow parallel to a ridge of hills that run in the x-direction, large-scale eddies impinge on the undulating surface and produce variations in the y and z directions in the normal stresses. The curl of these normal stresses, $\partial^2(\Delta\tau_{22} - \Delta\tau_{33})/\partial x \partial y$, produces a weak mean circulation with mean velocity of $O((H/L)u_0)$, and mean vorticity over a vertical scale of order L parallel to the crests of the hills (Wong 1985, Kretenauer & Schumann 1992). Shear flows running parallel to hills or waves are likely to produce a similar effect, and thence mean circulation, through a mechanism similar to the one that causes secondary flows in the corners of ducts or edges of plates first described by Prandtl (Townsend 1976, Section 7.20). Surface stress caused by these secondary flows may well contribute to the formation of seif dunes in sand that sometimes run parallel to the wind (e.g. Bagnold 1984).

6. SEPARATED FLOWS AND DOWNSTREAM WAKES

So far we have considered linear and weakly nonlinear processes caused by hills and waves with low slopes. When the slopes are steep, different, strongly nonlinear, phenomena become important. In the lee of a hill, downwind of the crest, the mean wind speed decreases and, if the slope of the hill is large enough, the mean near-surface wind decreases to such an extent that the mean-velocity gradient reverses. Consequently the mean-velocity gradient at the surface has to be zero at certain *critical points* where both the mean velocity and its gradient is zero. At least some of these critical points must be separation points, where streamlines leave the surface (Tobak & Peake 1982). Over two-dimensional hills, if the mean flow is also two dimensional, the same mean streamline connects the upstream and downstream critical points, namely *separation* and *attachment* points, thus forming a closed *separated-flow region*. Steep windward slopes can induce separation upwind of the crest, e.g. upwind of steep sand dunes (Barndorff-Neilson & Willetts 1991).

For typical hills with low slopes, $H/L \lesssim 0.3$, the thickness of any separated-flow region is comparable with the thickness of the inner region l_i, as in the Askervein experiment (e.g. Taylor & Teunissen 1987). In this case, flow in the outer region is not changed significantly, in the same way that the overall flow over the leading edge of an aircraft wing is not ruptured by a thin "separation bubble" within the boundary layer. So, to a first approximation, the surface-stress and the surface-pressure perturbations remain related by Equation 19. Then as the slope increases, and for large $\ln(l_i/z_0)$, the flow tends to separate, i.e. $\tau_B + \Delta\tau = 0$, toward the location where Δp is largest, namely about half way down a typically rounded isolated hill. For finite values of $\ln(l_i/z_0)$, the separation point moves up nearer the crest. This is consistent with Neish & Smith's (1992) asymptotic theory for flow around bluff bodies, which suggests that the separation point tends to the rear stagnation point as $\ln(l_i/z_0) \to \infty$. When the hills are rougher or when the approach flow is more sheared, Equation 19 shows that the stress perturbation has larger magnitude, so that separation tends to occur at smaller slopes. Experimental and numerical data in conjunction with these linear and weakly nonlinear concepts have led to useful practical estimates for the onset and location of separation as the slope and shape of the hill varies (Tampieri 1987, Wood 1995). In contrast to these characteristics of separation in turbulent flows, Equation 20 shows that in a high Reynolds number laminar flow separation tends to occur first where $\partial\Delta p/\partial x$ is greatest, namely near of the top of an isolated hill, as it does on a circular cylinder (Achenbach 1968).

Returning to turbulent flow, as the slope steepens the depth of the separated-flow region becomes comparable with the height H of the hill and extends a distance L_R downwind. This reattachment length L_R ranges from up to $12H$ for very smooth hills with steep slopes and low turbulence to about $6H$ if the downwind slope is greater than unity. L_R can decrease to as low as $3H$ for very turbulent flows and unevenly sloped or three-dimensional hills (Arya et al 1987).

Separated flows over hills, as with those over aircraft wings and bluff bodies (e.g. Lighthill 1963, Tobak & Peake 1982), are seldom precisely two dimensional or axisymmetric with closed streamlines. In fact, most separated regions in flow over hills are open, so that mean streamlines from the approach flow enter and leave the separated-flow regions, although they may recirculate several times within them. Thus the concept, advanced in the earliest papers, of a separated-flow region with closed streamlines and a separation bubble is not really appropriate. However, contaminants in some flows do tend to behave as if they are trapped because the recirculating streamlines delay downwind transport and dispersion for a time scale of about $3L_R/U_B(H)$ (e.g. Humphries & Vincent 1976, Hunt et al 1978).

It is observed in wind tunnels and water flumes that even if the hill is two dimensional, steep upwind slopes lead to flow patterns that vary in the cross-wind direction and that this is a result of vertical and longitudinal vortices being generated in the separated-flow regions upwind or downwind of the hill crest. Their origin appears to be a basic instability in which perturbations to the mean vorticity are stretched by the vertical and horizontal straining motion (e.g. Jackson 1973). The mechanism is, we believe, similar to that explored by Phillips et al (1996), discussed in Section 5.

Air leaving the separation point on steep leeward slopes of three-dimensional hills also tends to cause swirling flow far downwind of the hill (e.g. Jenkins et al 1981). The sense of the swirl (or sign of the vorticity ω_x) is more determined by the angle between the separation line and the incident flow than by the shear in the incident flow (cf. Mason & Morton 1987 and Hawthorne & Martin 1955). In weak turbulence, these vortices can persist far downwind and can distort the mean vorticity ω_y of the boundary layer. The result is that, in contrast to the usual wake behavior when the streamwise mean velocity is reduced, the streamwise mean velocity is actually increased (Kothari et al 1986). Again strong turbulence can disrupt these vortices.

Calculating turbulent wake flows downwind of hills in turbulent flows requires a model for the Reynolds stresses in relaxing shear layers in the presence of strong external turbulence, with initial conditions defined by the intermittent and large-scale eddies in the separated-flow region. One might argue that, in these complex situations, simple models are not appropriate, but when used carefully simple models can give useful results. For example, Counihan et al (1974) and Arya et al (1987) have found that data from wind tunnel and some field experiments for the downwind variation of the maximum velocity deficit $(-\Delta u)_m$ followed a power law decay

$$(-\Delta u)_m / U_B(H) \propto (x/H)^{-m}.$$

In two-dimensional wakes downwind of hills with low slopes and no separated-flow region, the data typically show $m \approx 2.0$, which follows using the mixing-length model (Equation 10). In two-dimensional wakes downwind of hills (and other obstacles) where the separated-flow region extends to the hill top, data show $m \approx 1.0$, which follows from calculations using Prandtl's mixing-length model for free shear layers, namely a constant mixing length (Counihan et al 1974). For separated three-dimensional flows $m \approx 1.5$. Recently, several authors calculated these or similar wake flows using closure models (e.g. Bonin et al 1995) and direct numerical simulation (Le et al 1997).

As explained in Section 4.1, whenever the flow over a wave contains a critical height, where $\overline{U}_B = 0$, there is reversed flow near the surface below the critical height. Hence the usual way of identifying separated flow by the presence of reversed flow requires modification. Identification of the critical points where the mean velocity and the velocity gradient are both zero remains the key to understanding, because they define the topology of the streamlines. When the wave amplitude is small, the recirculation associated with the critical layer lies entirely within the air flow, with two stagnation points, where the velocity is zero, lying on the critical height (Figure 4). Numerical simulations with an eddy viscosity suggest that, as the wave amplitude is increased, there remains just these two stagnation points even for steep waves (Gent & Taylor 1977). The streamline topology, therefore, remains the same, there are no critical points, and the flow is not separated. Hence, although the velocity gradient and surface stress may become zero at the wave surface, the surface velocity remains nonzero there: it remains determined by motions in the water. The air-flow streamline topology is changed when there is a critical point at the wave surface (Figure 6), which Banner & Melville (1976) show is associated with the onset of wave breaking. The overall shape of the wave surface is then affected, with a sharp change in wave slope near the crest (Banner & Peregrine 1993). This local geometrical discontinuity in slope affects the statistical description of the wave surface in terms of its spectrum (Belcher & Vassilicos 1997). Maat & Makin (1992) calculated the mean flow, shear stresses, and pressure field over a simple model of a breaking wave using an eddy viscosity to parameterize the stress, and showed a large increase in the asymmetry of the flow comparable to measurements of Banner (1990).

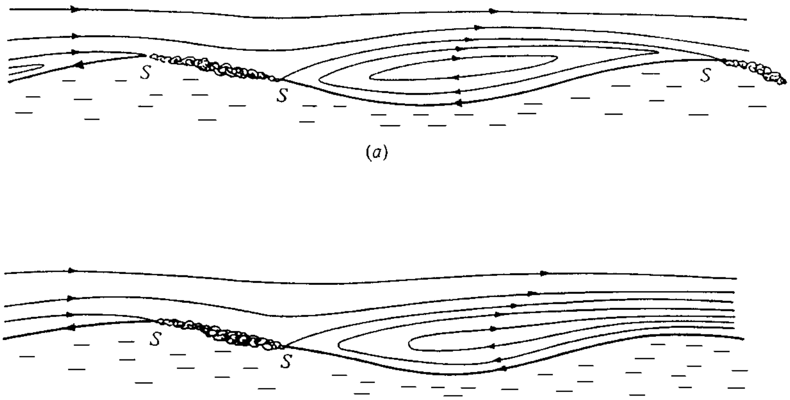

Figure 6 Conjectured mean streamlines for air flow over a breaking wave if the downwind wave is (*a*) breaking and (*b*) not breaking. Points marked *S* are critical points. (From Banner & Melville 1976).

7. ESTIMATES OF DRAG ON HILLS AND GROWTH OF WAVES

Over level terrain, the drag on the surface per unit area is $F_0 = u_*^2$. A hill induces additional drag ΔF per unit area, which is evaluated by integrating the stress over the surface of the hill, and can be separated into two components $\Delta F = \Delta F_p + \Delta F_\tau$, where

$$\Delta F_p = \frac{1}{\Lambda}\int_{Z=z_0} (\Delta p - \Delta\tau_{33})\sin\theta\,\mathrm{d}x, \quad \Delta F_\tau = \frac{1}{\Lambda}\int_{Z=z_0} \Delta\tau\cos\theta\,\mathrm{d}x, \tag{27}$$

and where $\tan\theta = Hdf/dx$, and Λ is an appropriate averaging length (e.g. the hill's wavelength). ΔF_τ is the *frictional drag*. ΔF_p is the *form drag*, which results from the component of the pressure perturbation that is correlated with the slope of the hill, Hdf/dx, i.e. the pressure associated with the asymmetric part of the perturbed flow. The contribution to ΔF_p from $\Delta\tau_{33}$ is small (Newley 1985).

Upper bounds for the two components of the drag can be found for hills with low slope, namely

$$\Delta F_p \le |\Delta p_{max}||\sin\theta_{max}| \sim \frac{H^2}{L^2}U_B^2(L),$$

$$\Delta F_\tau \le |\Delta\tau_{max}| \sim \frac{H}{L}\frac{U_B^2(L)}{U_B^2(l_i)}u_*^2. \tag{28a, b}$$

Growth of traveling surface waves, with surface elevation $\zeta' = \mathrm{Re}\{ae^{\mathrm{i}k(x'-ct')}\}$, of low slope, $ak \ll 1$, and with energy input given by the rate of working of the surface forces, $\dot{E}$ per unit wavelength, is governed by $\dot{E} = \dot{E}_p + \dot{E}_\tau$ (e.g. Belcher & Hunt 1993), where

$$\dot{E}_p = \int_{Z=z_0} (\Delta p - \Delta\tau_{33})\, \partial\zeta/\partial t\, \mathrm{d}x, \quad \dot{E}_\tau = \int_{Z=z_0} \Delta\tau\, \Delta u|_{z_0} \mathrm{d}x. \tag{29}$$

Since for a quasi-steady traveling wave $\partial\zeta'/\partial t' = -c\partial\zeta'/\partial x'$, it is the asymmetric part of the pressure that controls $\dot{E}_p$. The contribution from $\Delta\tau_{33}$ is small for all wave speeds (e.g. Mastenbroek 1996). The surface shear stress that is correlated with the surface-velocity perturbation contributes to $\dot{E}_\tau$. Notice that an explicit model is needed for the water motions before $\dot{E}_\tau$ can be evaluated, whereas the $\dot{E}_p$ can be evaluated for any wave motion. A low-amplitude gravity wave in deep water has energy per unit wavelength $E = \frac{1}{2}\rho_w g a^2$ and $\Delta u|_{z_0} = akc_r \cos\theta$, and the two contributions to $\dot{E}$ normalized on E have the following upper bounds

$$\frac{\dot{E}_p}{E} \lesssim 2\frac{\rho_a}{\rho_w}\frac{\{U_B(L) - c_r\}^2}{c_r^2} kc_r, \quad \frac{\dot{E}_\tau}{E} \lesssim 2\frac{\rho_a}{\rho_w}\frac{u_*^2}{c_r^2} kc_r. \tag{30a, b}$$

More refined estimates require estimates for the asymmetrical components of the flow.

7.1 *Estimates of Drag on Hills*

A number of mechanisms have been proposed that can lead to asymmetric components of flow over hills and waves. Jeffreys (1925) first proposed the *sheltering effect*, wherein the airflow separates. Neither his photographs of waves on Newnham Mill pond nor the low observed values of the wave growth rate supported this hypothesis. Ursell (1956) concluded that this proposal was discredited. However, as explained by Benjamin (1959) and in Section 3, a net drag can be caused by a sheltering effect even though the flow is not separated. Hence the term *nonseparated sheltering* (Belcher et al 1993) has been used to describe the mechanism whereby turbulent stresses in the boundary layer decelerate the air flow near the surface at the crest of the hill or wave leading, as explained in Section 3, to an asymmetric displacement, $\delta_\tau(x)$, that lead to (Sykes 1980, Belcher et al 1993)

$$\Delta F_p \sim \frac{H}{L} U_B^2(L) \frac{\delta_\tau}{L} \sim \frac{H^2}{L^2} \frac{U_B^4(L)}{U_B^4(l_i)} u_*^2, \tag{31}$$

which is a factor $u_*^2/U_B^2(L)$ smaller than the maximum estimate made by Jeffreys (1925). Changes to the turbulent normal stresses induced by the mean straining motions also contribute to Δp and thence the drag on hills or growth

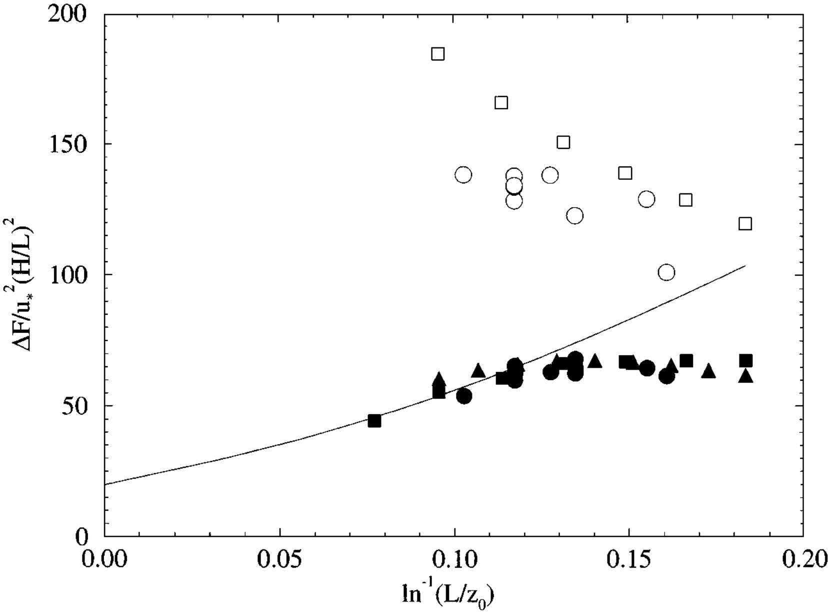

Figure 7 Drag on sinusoidal hills showing that models that correctly account for rapid distortion in the outer region (*filled symbols* and *line*) lead to smaller drag than models based on eddy-viscosity throughout the flow (*open symbols*). *Solid line*: linear theory for non-separated sheltering (Equation 31); *filled circles*: nonlinear numerical model with second-order closure; *open circles*: nonlinear numerical model with mixing-length closure (all from Belcher et al 1993); *filled squares*: nonlinear numerical model with second-order closure; *open squares*: nonlinear numerical model with mixing-length closure (from Mastenbroek 1996); *filled triangles*: linear numerical model with damped eddy-viscosity closure (Harris et al 1996).

of waves as explained in Section 5. Belcher et al (1993) showed that this mechanism acting in the outer and inner regions contributes $\Delta F_p \sim (H/L)^3 u_*^2$, $(H/L)^2 u_*^2/\ln(l_i/z_0)$, which, for low slopes and smooth surfaces, are much smaller than the nonseparated sheltering. Figure 7 shows that different methods for calculating the drag compare well, provided the rapid-distortion regions are accounted for. It also shows that, if an eddy-viscosity model is inappropriately used in the outer region the drag would be overestimated by a factor $U_B(L)/u_*$ (e.g. Jacobs 1987, van Duin & Janssen 1992), because the shear stress in the outer region then leads to asymmetry in addition to the asymmetry in the inner region (Belcher et al 1993).

Wood & Mason (1993) showed that the linear result (Equation 31) can be extended to drag on three-dimensional hills by dividing the hill into thin slices parallel to the flow, calculating the drag on each slice using the results for two-dimensional hills, and then summing over slices. Mason (1985) argued that when the slopes of the hills are steep, the hill acts as a bluff body, so that the drag is approximately equal to the maximum estimate given by Equation 28a. Wood & Mason (1993) obtained an estimate for the drag coefficient over the whole range of slopes and for two-dimensional and three-dimensional hills by switching from the low-slope estimate (Equation 31) to the bluff-body estimate (Equation 28a) at a critical value of the hill slope. Their resulting formula for the drag showed excellent agreement with values computed from nonlinear numerical simulations.

The resulting formula for the drag is now used for parameterizing the subgrid-scale contribution to the drag of hills in NWP models. Observations of boundary layers over hilly terrain show that the areally averaged velocity profile, $\langle U \rangle$, is approximately logarithmic (e.g. Nappo 1977, Grant & Mason 1990), namely

$$\langle U \rangle \approx \left(u_*^{\mathrm{eff}}/\kappa\right) \ln\left((z - d^{\mathrm{eff}})/z_o^{\mathrm{eff}}\right), \tag{32}$$

where $(u_*^{\mathrm{eff}})^2$ is the total surface stress including the form drag, and z_0^{eff} and d^{eff} are the *effective roughness length* and *effective displacement height* of the hills (Mason 1985, Taylor et al 1989). Mason & Wood (1993) explained that their formula for the drag can be used to compute this effective roughness length and found that the ratio z_0^{eff}/H showed systematic variation with the shape and properties of the hills and lay in the range 10^{-3} to 10^{-1}, which is of similar magnitude to the usual "rule of thumb" that the roughness length is $\frac{1}{30}$ of the height of the roughness elements.

7.2 *Growth of Waves*

Figure 8 shows variation of measured and calculated values of the growth-rate coefficient, β, defined by $\dot{E}/E = (\rho_a/\rho_w)(u_*/c_r)^2\beta\, kc_r$, with the wind and wave speeds, c_r/u_*. Understanding the variation of the model curves follows from the understanding of the asymmetry in the flow in each of the wind–wave regimes.

As explained in Section 4.3, in the slow-wave regime, $c_r/u_* \lesssim 15$, asymmetry in the flow has the same form as in flow over a hill. The growth rate from the nonseparated sheltering then becomes (Belcher & Hunt 1993)

$$\frac{\dot{E}_p}{E} \sim 2\frac{\rho_a}{\rho_w}\frac{\{U_B(L) - c_r\}^2}{c_r^2} kc_r k\delta_\tau \sim 2\frac{\rho_a}{\rho_w}\frac{u_*^2}{c_r^2}\frac{U_B^4(L)}{U_B^4(l_i)} kc_r. \tag{33}$$

This has the same magnitude as the contribution from the surface stresses; although detailed computations show that the stress contribution is numerically smaller (Mastenbroek 1996). Just as with calculations of drag on hills, if a mixing length is used erroneously in the outer region, then Equation 33 would

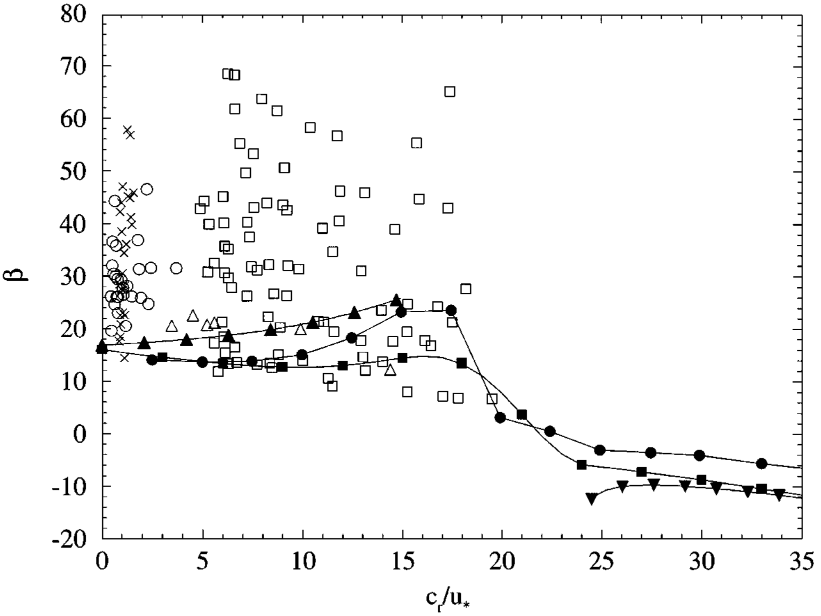

Figure 8 Variation of wave growth-rate coefficient with c_r/u_* when $kz_0 = 10^{-4}$. *Filled upward-pointing triangles*: linear theory for slow waves (Belcher & Hunt 1993); *filled downward-pointing triangles*: linear theory for fast waves (Cohen 1997); *filled squares*: linear numerical model with damped mixing-length closure (Cohen 1997); *filled circles*: nonlinear numerical model with second-order closure (Mastenbroek 1996); *other symbols*: data collated by Plant (1984).

be larger by a factor of $U_B(L)/u_*$ (Jacobs 1987, van Duin & Janssen 1992). As c_r/u_* increases, the depth of the inner region, and hence asymmetry from sheltering, increases, so that the growth rate increases, as shown in Figure 8. Additional asymmetry, and hence contribution to growth, is generated by the critical layer for growing slow waves, with $c_i/u_* \ll 1$, but this contribution is smaller than from the sheltering (Miles 1993, 1996). For slow waves, the critical layer lies within the inner surface layer, where the Reynolds shear stress dominates, and quantitative estimates for its contribution to growth might be smaller than the value from Miles' (1957) inviscid theory.

Following the qualitative reasoning given in Section 4.3, we expect that across the intermediate regime, where $15 \lesssim c_r/u_* \lesssim 25$, the contribution to wave growth from sheltering increases, reaches a maximum, and then reduces to negative values as the negative sheltering from the reverse flow below the critical height becomes larger than the positive sheltering. According to Miles (1957, Figure 1) the critical-layer contribution to growth increases with kz_c to a maximum when $kz_c \approx 10^{-2}$, which implies $c_r/u_* \approx 12$, and then falls rapidly to zero. The overall growth rate therefore increases and reaches a maximum at $c_r/u_* \approx 15$ and then becomes negative, as is indeed seen in the computed results shown in Figure 8.

In the fast-wave regime, where $c_r/U_B(L) \gtrsim 1$ so that $kz_c \gtrsim 1$, shear in U_B at z_c is too small for the critical layer to contribute significantly to growth. Negative sheltering from the reverse flow below the critical height and asymmetries from the orbital velocities at the wave surface both lead to negative growth, i.e. damping, rates of the same form as Equation 33 (Cohen 1997) (Figure 8). But Equation 33 shows that the time scale for damping of fast waves is much longer than the time scale for growth of slow waves because c_r/u_* is much larger for fast waves; hence fast waves, which frequently arise as swell, interact only weakly with wind.

The growth rate given by Equation 33 has the same form as found by examining data (Plant 1981), but the coefficient obtained from theory is a factor of two to three smaller than the coefficient derived from the measurements, particularly at small c_r/u_*, as shown in Figure 8. So what is wrong? Variation in roughness along the wave might significantly change flow in the lee (as Britter et al 1981 observed for hills); and, larger roughness near the crest does increase the sheltering and thence the growth rate (Gent & Taylor 1976). But Mastenbroek (1996) developed a comprehensive model of how roughness from a spectrum of short waves varies along a long wave, allowing for wind-input to, and advection of, the short waves, and found that growth of the long wave is increased by only 50%. This is smaller than the required 200–300% to bring theory into line with the data.

Although only a small fraction of ocean waves are breaking (something like 5%), their violent effect on the air flow may explain the discrepancy between observations and theory of growth rates (Banner 1990). As explained in Section 6.2, wave-breaking provokes air flow separation, so that asymmetry in the air flow increases sufficiently that the wave growth rate becomes closer to its maximum value (Equation 7.4) suggested by Jeffreys (1925), which is then of the form suggested by Snyder et al (1974) based on ocean data. A significant fraction of strongly forced waves, i.e. small c_r/u_*, break (Donelan et al 1985, Figure 19), so this might explain the large difference between theory and data at small c_r/u_* less than about 5 (Figure 8). But for larger values of c_r/u_*, more typical of the ocean, a smaller fraction break, and it is not yet clear whether the average effect of breaking is significant.

An estimate of the total drag of the sea surface, or its effective roughness length, z_0^{eff}, is obtained if the form drag on each sinusoidal wave component is integrated over the spectrum of waves. Makin et al (1995) find that the drag is largely determined by short waves with wavelengths in the range 1 cm to 5 m. The effective roughness is of the form $z_0^{\text{eff}} = \alpha_c (u_*^{\text{eff}})^2/g$, which is of the form proposed by Charnock (1955) on dimensional grounds. The Charnock parameter is $\alpha_c \approx 0.010 - 0.19$, and there remains debate over whether or not it depends on sea state (Donelan et al 1993, Yelland & Taylor 1996).

8. CONCLUSIONS

There are many applications of modeling air flow over hills and waves, some of which we mentioned in the introduction. For practical purposes, what is needed is clear physical insight into the physical mechanisms, their orders of magnitude, and their ranges of application. Current models do not represent several of the mechanisms described here, particularly those associated with the secondary motions described in Section 5. But these are, arguably, less significant in applications with strong turbulence. However, they may affect mass transfer, e.g. in the location of maximum transport. There remain interesting challenges in modeling air flow over waves—for example air flow over a group of waves or when a front of waves propagates into still water. These are both spatially nonhomogeneous wave systems that require new experiments such as those of Chu et al (1992) and new theoretical ideas such as proposed by McIntyre (1996). Air flow on the lee side of the hills or waves is obviously important, yet separated and relaxing turbulent wake flows are still not satisfactorily modeled. Large-eddy simulation might give useful insights, although careful resolution of the inner region will be costly. Finally, there remain interesting phenomena that couple turbulent motions in air and water that depend on the relative strengths of the turbulence in the two fluids.

Literature Cited

Achenbach EL. 1968. Distribution of local pressure and skin friction around a circular cylinder in cross-flow up to $Re = 5 \times 10^6$. *J. Fluid Mech.* 34:625–39

Arya SPS, Capuano ME, Fagne LC. 1987. Some fluid modelling studies of flow and dispersion over two-dimensional low hills. *Atmos. Env.* 21:753–64

Bagnold RA. 1984. *The Physics of Blown Sand and Desert Dunes*. London: Chapman & Hall

Banner ML. 1990. The influence of wave breaking on the surface pressure distribution in wind–wave interactions. *J. Fluid Mech.* 211:463–95

Banner ML, Melville WK. 1976. On separation of air flow over water waves. *J. Fluid Mech.* 77:825–42

Banner ML, Peregrine DH. 1993. Wave breaking in deep water. *Annu. Rev. Fluid Mech.* 25:373–97

Barndorff-Nielson OE, Willetts BB. 1991. Aeolian grain transport. II: The erosional environment. *Acta Mech.* 2 (Suppl.)

Batchelor GK, Proudman I. 1954. The effect of rapid distortion on a fluid in turbulent motion. *Q. J. Mech. Appl. Math.* 7:83–103

Belcher SE, Hunt JCR. 1993. Turbulent shear flow over slowly moving waves. *J. Fluid Mech.* 251:109–48

Belcher SE, Newley TMJ, Hunt JCR. 1993. The drag on an undulating surface due to the flow of a turbulent boundary layer. *J. Fluid Mech.* 249:557–96

Belcher SE, Vassilicos JC. 1997. Breaking waves and the equilibrium range of wind-wave spectra. *J. Fluid Mech.* 342:377–401

Benjamin TB. 1959. Shearing flow over a wavy boundary. *J. Fluid Mech.* 6:161–205

Beryland ME. 1972. Atmospheric diffusion investigations in the U.S.S.R. *W.M.O. Tech. Note 121*

Bonin JC, Buchal T, Rodi W. 1995. ERCOFTAC workshop on data bases and testing of calculation methods for turbulent flows. *ERCOFTAC Bull.* pp. 48–54

Bradshaw P, Ferris DH, Atwell NP. 1967. Calculation of boundary layer development using the turbulent kinetic energy equation. *J. Fluid Mech.* 28:593–616

Britter RE, Hunt JCR, Richards KJ. 1981. Air flow over a 2-d hill: studies of velocity speed-up, roughness effects and turbulence. *Q. J. R. Meteorol. Soc.* 107:91–110

Building Research Establishment. 1989. The assessment of wind speed over topography. *Build. Res. Establ. Dig. 346*

Burgers G, Makin VK. 1993. Boundary-layer model results for wind-sea growth. *J. Phys. Oceanog.* 23:372–85

Carruthers DJ, Choularton TW. 1983. A model of the seeder-feeder mechanism of orographic rain including stratification and wind-drift effects. *Q. J. R. Meteorol. Soc.* 109:575–88

Castro IP, Snyder WH. 1982. A wind-tunnel study of dispersion from sources downwind of three-dimensional hills. *Atmos. Env.* 16:1869–87

Choularton TW, Perry SJ. 1986. A model of the orographic enhancement of snowfall by the seeder-feeder mechanism. *Q. J. R. Meteorol. Soc.* 112:335–45

Chu JS, Long SR, Phillips OM. 1992. Measurements of the interaction of wave groups with shorter wind-generated waves. *J. Fluid Mech.* 245:191–210

Cohen JE. 1997. *Theory of turbulent wind over fast and slow waves*. PhD Thesis. Univ. Cambridge. 228 pp.

Counihan J, Hunt JCR, Jackson PS. 1974. Wakes behind two-dimensional surface obstacles in turbulent boundary layers. *J. Fluid Mech.* 64:529–63

Craik ADD. 1982. Wave-induced longitudinal-vortex instability in shear flows. *J. Fluid Mech.* 125:37–52

Donelan MA, Hamilton J, Hui WH. 1985. Directional spectra of wind-generated waves. *Philos. Trans. R. Soc. London* 315:509–62

Donelan MA, Dobson FW, Smith SD, Anderson RJ. 1993. On the dependence of sea surface roughness on wave development. *J. Phys. Oceanog.* 23:2143–49

Fuller SR, Kellett SA. 1997. *Annual Forecast Verification Statistics 1996.* Bracknell, UK: Meteorological Office

Gent PR, Taylor PA. 1976. A numerical model of air flow above water waves. *J. Fluid Mech.* 77:105–28

Gent PR, Taylor PA. 1977. A note on “separation” over short wind waves. *Boundary Layer Met.* 11:65–87

Gong WM, Taylor PA, Dornbrack A. 1996. Turbulent boundary-layer flow over fixed aerodynamically rough two-dimensional sinusoidal waves. *J. Fluid Mech.* 312:1–37

Grant ALM, Mason PJ. 1990. Observations of boundary-layer structure over complex terrain. *Q. J. R. Meteorol. Soc.* 116:159–86

Harris JA, Belcher SE, Street RL. 1996. Linear dynamics of wind waves in coupled turbulent air–water flow: Part 2. *J. Fluid Mech.* 308:219–54

Hasselmann K. 1962. On the nonlinear energy transfer in a gravity wave spectrum: Part 1. *J. Fluid Mech.* 12:481–500

Hawthorne WR, Martin ME. 1955. The generation of secondary vorticity in the flow over a hemisphere due to density gradient and shear. *Proc. R. Soc. London Ser. A* 232:184–95

Hewer FE, Wood N. 1998. The effective roughness length for scalar transfer in neutral conditions over hilly terrain. *Q. J. R. Meteorol. Soc.* In press

Humphries W, Vincent JH. 1976. An experimental investigation of the detention of airborne smoke in the wake bubble behind a disk. *J. Fluid Mech.* 73:453–64

Hunt JCR. 1973. A theory of turbulent flow round two-dimensional bluff bodies. *J. Fluid Mech.* 61:625–706

Hunt JCR, Abell CJ, Peterka JA, Woo H. 1978. Kinematical studies of the flows around free or surface-mounted obstacles: applying topology to flow visualisation. *J. Fluid Mech.* 86:179–200

Hunt JCR, Leibovich S, Richards KJ. 1988. Turbulent shear flows over low hills. *Q. J. R. Meteorol. Soc.* 114:1435–70

Hunt JCR, Richards KJ. 1984. Stratified airflow over one or two hills. *Boundary-Layer Meteorol.* 30:223–59

Hunt JCR, Tampieri F, Weng WS, Carruthers DJ. 1991. Air-flow and turbulence over complex terrain—a colloquium and a computational workshop. *J. Fluid Mech.* 227:667–88

Jacobs SJ. 1987. An asymptotic theory for the turbulent flow over a progressive wave. *J. Fluid Mech.* 174:69–80

Jackson PS. 1973. *Flow around obstacles in boundary layers*. PhD Thesis. Univ. Cambridge

Jackson PS, Hunt JCR. 1975. Turbulent wind flow over a low hill. *Q. J. R. Meteorol. Soc.* 101:929–55

Janssen PAEM. 1982. Quasilinear approximation for the spectrum of wind generated ocean waves. *J. Fluid Mech.* 117:493–506

Jeffreys H. 1925. On the formation of water waves by wind. *Proc. R. Soc. London Ser. A* 107:189–206

Jenkins GJ, Mason PJ, Moores WH, Sykes RI. 1981. Measurements of the flow structure around Ailsa Craig, a steep three-dimensional isolated hill. *Q. J. R. Meteorol. Soc.* 107:833–51.

Komen GJ, Cavaleri L, Donelan MA, Hasselmann K, Hasselmann S, Janssen PAEM. 1994. *Dynamics and Modelling of Ocean Waves*. Cambridge: Cambridge Univ. Press

Kothari KM, Peterka JA, Meroney RN. 1986. Perturbation analysis and measurements of building wakes in a stably stratified turbulent boundary layer. *J. Wind Eng. Ind. Aero.* 25:49–74

Krettenauer K, Schumann U. 1992. Numerical simulation of turbulent convection over wavy terrain. *J. Fluid Mech.* 237:261–99

Launder BE. 1989. Second moment closure: Present and future. *Int. J. Heat Fluid Flow* 10:282–99

Launder BE, Reece GT, Rodi W. 1975. The development of a Reynolds stress turbulent closure. *J. Fluid Mech.* 68:537–66

Le H, Moin P, Kim J. 1997. Direct numerical simulation of turbulent flow over a backward facing step. *J. Fluid Mech.* 330:375–409

Lighthill MJ. 1962. Physical interpretation of the theory of wind generated waves. *J. Fluid Mech.* 14:385–97

Lighthill MJ. 1963. Attachment and separation in three-dimensional flows. In *Laminar Boundary Layers*, ed. L Rosenhead, Ch. 2, pp. 72–82. Oxford: Oxford Univ. Press

Maat N, Makin VK. 1992. Numerical simulation of air-flow over breaking waves. *Boundary-Layer Meteorol.* 60:77–93

Makin VK, Kudryatsev VN, Mastenbroek C. 1995. Drag of the sea surface. *Boundary-Layer Meteorol.* 73:159–82

Mason PJ. 1985. On the parameterisation of orographic drag. In *Proc. ECMWF Sem. Phys. Paramet. Numer. Models Atmos., Reading*, pp. 139–165. Reading, UK: ECMWF

Mason PJ, King JC. 1985. Measurements and predictions of flow and turbulence over an isolated hill of moderate slope. *Q. J. R. Meteorol. Soc.* 111:617–40

Mason PJ, Morton BR. 1987. Trailing vortices in the wakes of surface-mounted obstacles. *J. Fluid Mech.* 175:247–93

Mason PJ, Sykes RI. 1979. Flow over an isolated hill of moderate slope. *Q. J. R. Meteorol. Soc.* 105:383–95

Mason PJ, Sykes RI. 1980. A two-dimensional numerical study of horizontal roll vortices in the neutral atmospheric boundary layer. *Q. J. R. Meteorol. Soc.* 106:351–66

Mastenbroek C. 1996. *Wind–wave interaction*. PhD Thesis. Delft Tech. Univ. 119 pp.

Mastenbroek C, Makin VK, Garat MH, Giovanangeli JP. 1996. Experimental evidence of the rapid distortion of turbulence in air flow over waves. *J. Fluid Mech.* 318:273–302

McIntyre ME. 1993. On the role of wave propagation and wave breaking in atmosphere–ocean dynamics. *Proc. Int. Cong. Theoret. Appl. Mech., 18th, Haifa*, pp. 281–304. Amsterdam: Elsevier

Messiter AF. 1979. Boundary-layer separation. *Proc. US Natl. Appl. Mech. Congr., 8th, Los Angeles*, pp. 157–79. See also: Boundary layer interaction theory. *Trans. ASME J. Appl. Mech.* 50:1104–34 (1983)

Miles JW. 1957. On the generation of surface waves by shear flows. *J. Fluid Mech.* 3:185–204

Miles JW. 1993. Surface wave generation revisited. *J. Fluid Mech.* 256:427–41

Miles JW. 1996. Surface wave generation: a viscoelastic model. *J. Fluid Mech.* 322:131–45

Milton SF, Wilson CA. 1996. Impact of parameterised subgrid-scale orographic forcing on systematic errors in a global NWP model. *Mon. Weather Rev.* 124:2023–45

Nappo CJ. 1977. Mesoscale flow over complex terrain during the Eastern Tenessee Trajectory Experiment (ETTEX). *J. Appl. Meteorol.* 16:1186–96

Neish A, Smith FT. 1992. On turbulent separation in the flow past a bluff body. *J. Fluid Mech.* 241:443–67

Newley TMJ. 1985. *Turbulent air flow over low hills*. PhD Thesis. Univ. Cambridge

Palmer TN, Shutts GJ, Swinbank R. 1986. Alleviation of a systematic westerly wind bias in general circulation and numerical weather prediction models through an orographic gravity wave drag parameterizaion. *Q. J. R. Meteorol. Soc.* 112:1001–39

Panofsky HA. 1974. The atmospheric boundary layer below 150 metres. *Annu. Rev. Fluid Mech.* 6:147–77

Phillips OM. 1977. *Dynamics of the Upper Ocean*. Cambridge: Cambridge Univ. Press

Phillips WRC, Wu Z, Lumley JL. 1996. On the formation of longitudinal vortices in a turbulent boundary-layer over wavy terrain. *J. Fluid Mech.* 326:321–41

Pielke RA. 1984. *Mesoscale Meteorological Modelling*. London: Academic

Plant WJ. 1984. A relationship between wind shear stress and wave slope. *J. Geophys. Res.* 87(C3):1961–67

Prandtl L. 1960. *Essentials of Fluid Mechanics*. London: Blackie

Raupach MR, Weng WS, Carruthers DJ, Hunt

JCR. 1992. Temperature and humidity fields and fluxes over low hills. *Q. J. R. Meteorol. Soc.* 118:191–225

Smith FT, Brighton PMW, Jackson PS, Hunt JCR. 1981. On boundary layer flow past two dimensional bodies. *J. Fluid Mech.* 113:123–52

Snyder RL, Dobson FW, Elliot JA, Long RB. 1981. Array measurements of atmospheric pressure fluctuations above gravity waves. *J. Fluid Mech.* 102:1–59

Stewartson K. 1974. Multi-structured boundary layers on flat plates and related bodies. *Adv. Appl. Math.* 14:145–239

Sykes RI. 1980. An asymptotic theory of incompressible turbulent flow over a small hump. *J. Fluid Mech.* 101:647–70

Tampieri F. 1987. Separation features of boundary layer flow over valleys. *Boundary Layer Meteorol.* 40:295–307

Taylor PA. 1977. Numerical studies of neutrally stratified planetary boundary layer flow above gentle topography. 1: 2-D cases. *Boundary-Layer Meteorol.* 12:37–60

Taylor PA, Sykes RI, Mason PJ. 1989. On parameterisation of drag over small-scale topography in neutrally-stratified boundary-layer flow. *Boundary-Layer Meteorol.* 48: 409–22

Taylor PA, Teunissen HW. 1987. The Askervien hill project: overview and background data. *Boundary-Layer Meteorol.* 39:15–39

Tennekes H, Lumley JL. 1972. *A First Course in Turbulence*. Cambridge: MIT Press

Tobak M, Peake DJ. 1982. Topology of three-dimensional separated flows. *Annu. Rev. Fluid Mech.* 14:61–85

Townsend AA. 1961. Equilibrium layers and wall turbulence. *J. Fluid Mech.* 11:97–120

Townsend AA. 1972. Flow in a deep turbulent boundary layer over a surface distorted by water waves. *J. Fluid Mech.* 55:719–35

Townsend AA. 1976. *The Structure of Turbulent Shear Flow*. Cambridge: Cambridge Univ. Press

Townsend AA. 1980. Sheared turbulence and additional distortion. *J. Fluid Mech.* 98:171–91

Troen I, Petersen EL. 1989. *The European Wind Atlas*. Roskilde, Denmark: Ris. Natl. Lab.

Ursell F. 1956. Wave generation by wind. In *Surveys in Mechanics*, ed. GK Batchelor, RM Davis, pp. 216–49. Cambridge: Cambridge Univ. Press

Van Duin CA. 1996. Rapid-distortion models in the theory of surface-wave generation. *J. Fluid Mech.* 329:147–53

Van Duin CA, Janssen PAEM. 1992. An analytical model of the generation of surface gravity waves by turbulent air flow. *J. Fluid Mech.* 236:197–215

Walmsley JL, Taylor PA. 1996. Boundary-layer flow over topography: impacts of the Askervein study. *Boundary-Layer Meteorol.* 78:291–320

Wong HYW. 1985. *Shear free turbulence and secondary flow near angled and curved surfaces.* PhD Thesis. Univ. Cambridge

Wood N. 1995. The onset of separation in neutral turbulent flow over hills. *Boundary-Layer Meteorol.* 76:137–64

Wood N, Mason PJ. 1993. The pressure force induced by neutral turbulent flow over hills. *Q. J. R. Meteorol. Soc.* 119:1233–67

Yelland M, Taylor PK. 1996. Wind stress measurements from the open ocean. *J. Phys. Oceanog.* 26:541–58

Zeman O, Jensen NO. 1987. Modification to turbulence characteristics in flow over hills. *Q. J. R. Meteorol. Soc.* 113:55–80

Annual Review of Fluid Mechanics
Volume 30, 1998

CONTENTS

Lewis Fry Richardson and His Contributions to Mathematics, Meteorology, and Models of Conflict, *J.C.R. Hunt*	0
Aircraft Laminar Flow Control , *Ronald D. Joslin*	1
Vortex Dynamics in Turbulence, *D. I. Pullin, P. G. Saffman*	31
Interaction Between Porous Media and Wave Motion, *A. T. Chwang, A. T. Chan*	53
Drop and Spray Formation from a Liquid Jet, *S. P. Lin, R. D. Reitz*	85
Airplane Trailing Vortices, *Philippe R. Spalart*	107
Diffuse-Interface Methods in Fluid Mechanics, *D. M. Anderson, G. B. McFadden, A. A. Wheeler*	139
Turbulence in Astrophysics: Stars, *V. M. Canuto, J. Christensen-Dalsgaard*	167
Vortex-Body Interactions, *Donald Rockwell*	199
Nonintrusive Measurements for High-Speed, Supersonic, and Hypersonic Flows, *J. P. Bonnet, D. Grésillon, J. P. Taran*	231
Renormalization-Group Analysis of Turbulence, *Leslie M. Smith, Stephen L. Woodruff*	275
Control of Turbulence, *John Lumley, Peter Blossey*	311
Lattice Boltzmann Method for Fluid Flows, *Shiyi Chen, Gary D. Doolen*	329
Boiling Heat Transfer, *V. K. Dhir*	365
Direct Simulation Monte Carlo--Recent Advances and Applications, *E.S. Oran, C.K. Oh, B.Z. Cybyk*	403
Air-Water Gas Exchange, *B. Jähne, H. Haußecker*	443
Computational Hypersonic Rarefied Flows, *M. S. Ivanov, S. F. Gimelshein*	469
Turbulent Flow Over Hills and Waves, *S. E. Belcher, J. C. R. Hunt*	507
Direct Numerical Simulation: A Tool in Turbulence Research, *Parviz Moin, Krishnan Mahesh*	539
Micro-Electro-Mechanical-Systems (MEMS) and Fluid Flows, *Chih-Ming Ho, Yu-Chong Tai*	579
Fluid Mechanics for Sailing Vessel Design, *Jerome H. Milgram*	613
Direct Numerical Simulation of Non-Premixed Turbulent Flames, *Luc Vervisch, Thierry Poinsot*	655